THE ASTROPHYSICAL JOURNAL, 355:197–209, 1990 May 20

SHOCKED [O I] 63 MICRON LINE EMISSION FROM THE SUPERNOVA REMNANT IC 443

MICHAEL G. BURTON,[1,2] D. J. HOLLENBACH,[1] M. R. HAAS,[1] AND E. F. ERICKSON[1]
Received 1989 May 22; accepted 1989 November 17

ABSTRACT

The [O I] $^3P_1 \rightarrow {}^3P_2$ fine-structure line at 63.18 μm has been observed at nine locations in a $1' \times 2'$ region in the supernova remnant (SNR) IC 443. Upper limits to the line emission from [Si II] $^2P_{3/2} \rightarrow {}^2P_{1/2}$ at 34.8 μm and CO ($J = 22$–21) at 118.6 μm have also been obtained. These are the first reported observations of far-infrared line emission from an SNR. The peak [O I] line flux occurs at the same location as the shock-excited molecular hydrogen emission peak. Comparison with the *IRAS* far-IR emission shows that the [O I] 63 μm line emission is an important contributor to the 60 μm band, with estimates ranging from $\sim$40%–75% of the total band flux. This is the first region of this type to be discovered in the *IRAS* data set. The distribution of the [O I] line emission appears to be similar to that of the molecular hydrogen 1–0 $S(1)$ line. We consider the possibility of X-ray or far-UV excitation of the emission, but we conclude that the [O I] line emission is shock-excited. The IR line emission is modeled using a variety of C and J shocks. We find, based on our current theoretical understanding of shock processes, that C shocks with a distribution of shock velocities from 10–45 km s^{-1} are present, with the lower velocity C shocks providing the [O I] 63 μm line emission and the higher velocity C shocks the 1–0 $S(1)$ line emission. This model *cannot*, however, explain why the [O I] 63 μm/H_2 1–0 $S(1)$ and H_2 1–0 $S(1)$/2–1 $S(1)$ line ratios appear to remain relatively constant across the source, unless the ad hoc assumption is made that the distribution of shock velocities is the same in every beam. However, by relaxing certain theoretical assumptions, a partially dissociative J shock model with $v_s \sim$ 10–20 km s^{-1} *can* explain the observations. It has to be assumed that both (1) the shock is indeed J type despite suspicions that the physical parameters of the flow are appropriate to C shocks and (2) the oxygen chemistry is suppressed so that H_2O and OH are not formed. We can offer little theoretical rationale for making these assumptions. Such a shock model has, however, been found by Brand *et al.* to provide an excellent fit to the H_2 line emission from OMC-1. The far-IR shocked line emission (O I, H_2O, CO) may well dominate the total emission in the *IRAS* bands, with [O I] 63 μm line emission dominating the 60 μm band, and with H_2O and/or CO line emission contributing appreciably to the 100 μm band. Thus, previous models involving collisionally heated grains to explain the *IRAS* emission from the shocked molecular region may be unnecessary.

Subject headings: infrared: spectra — nebulae: individual (IC 443) — nebulae: supernova remnants — shock waves

I. INTRODUCTION

Although many galactic supernova remnants (SNRs) are located near large molecular clouds, unequivocal evidence for the interaction of the supernova (SN) shock wave with these clouds remains confined to a few isolated examples. IC 443 provides the best known and most studied case.

A molecular cloud runs NW-SE across the face of the bubble defining the SNR in optical photographs, roughly bisecting the bubble into two lobes (Cornett, Chin, and Knapp 1977). The SN blast wave is interacting with different components of the interstellar medium (ISM) at various locations in the remnant, producing copious amounts of shocked line emission from ionized gas (e.g., Fesen and Kirshner 1980), atomic gas (e.g., Braun and Strom 1986*a*), and molecular gas (e.g., Burton *et al.* 1988; White *et al.* 1987), as well as continuum X-ray emission (e.g., Petre *et al.* 1983, 1988; Watson *et al.* 1983), far-infrared emission (e.g., Braun and Strom 1986*b*; Mufson *et al.* 1986), and radio emission (e.g., Erickson and Mahoney 1985; Mufson *et al.* 1986). In particular, shocked 2 μm line emission from H_2 has been observed (Burton *et al.* 1988; Burton 1987, 1988) arising from many bright peaks distributed along a narrow, sinuous ridge. The ridge forms a nearly complete ring, over 20 pc long ($\sim$45′), and it emits $\sim$1000 $L_\odot$ in the H_2 lines (mostly through rotational-vibrational transitions in the near-infrared), comparable to the $\sim$3700 $L_\odot$ of far-infrared emission measured by *IRAS* (mainly through the 60 + 100 μm bands; Mufson *et al.* 1986). High-velocity molecular line emission from OH, and from $J = 1$–0 CO, HCO^+, and HCN, has also been observed and partially mapped at radio wavelengths (DeNoyer 1979*a*, *b*; White *et al.* 1987), and high-velocity 21 cm H I line emission has been mapped by Braun and Strom (1986*a*). These high-velocity species presumably arise in the cold postshock gas relatively far downstream from the shock front, in contrast to the H_2 line emission, which is from hot, recently shocked material. The distribution of the line emission from all the shocked molecules and H I is remarkably similar (Burton *et al.* 1988). In Figure 1 we present an overlay of the *IRAS* 60 μm band and H_2 1–0 $S(1)$ line maps, together with the locations where we observed the 63 μm [O I] line. The figure also demonstrates that the overall distribution of the H_2 line and 60 μm band emission are similar.

The H_2 line ratios and the variety of high-velocity species observed provide clear evidence for the presence of a shock, driven into an associated molecular cloud by the expanding, high-pressure gas of a supernova remnant. In IC 443 the observations are uncontaminated by outflowing gas from a star-

[1] Space Science Division, NASA Ames Research Center.
[2] University of California at Irvine.

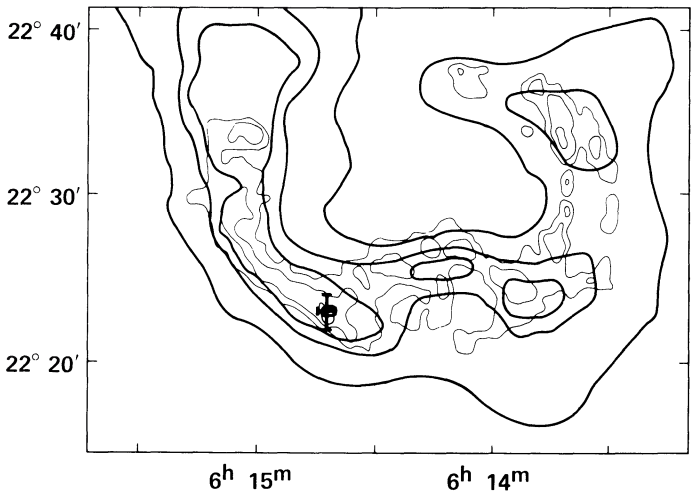

FIG. 1.—Overlay of maps of the H_2 1–0 $S(1)$ line (*light line*, from Burton 1988) and the *IRAS* 60 μm band (*heavy line*, from Braun and Strom 1986*b*) in IC 443. The region covered by the [O I] 63 μm line observations is shown by the cross.

forming region, by ionized gas in an H II region, or by warm atomic gas from a photodissociation region, thus providing an excellent laboratory for the investigation of molecular shocks. A comparison of the line emission from the various species enables a detailed study of shock waves inside a molecular cloud. Furthermore, comparison of the total intensity emitted in the various lines allows the energy budget of the shock to be calculated and the dominant coolant to be determined.

The presence of atomic gas, especially the large amounts of high-velocity H I, and molecular gas together in IC 443 suggests several possible shock models. The shocks may be, for instance, partially dissociative, leaving behind them a compressed shell of high-velocity molecular gas and dissociated atomic gas. Alternatively, shocks of varying velocity and preshock density, but with the same driving pressure, may fill the beam. In this picture, the faster shocks totally dissociate the H_2 while the slower shocks are essentially nondissociative. On the other hand, since the H I gas is probably cold material shocked prior to the infrared-emitting gas, it may be that decelerating shocks previously dissociated the H_2, but currently are nondissociative and only heat the H_2 and O I.

In this paper, we present observations of the 63.2 μm [O I] fine-structure line in IC 443, as well as upper limits to the line emission from CO $J = 22$–21 at 118.6 μm and from [Si II] at 34.8 μm. These are the first far-infrared observations of line emission from an SNR. The emission is well correlated with the H_2 emission, and we argue that it is shock-excited, like the H_2. Theoretical modeling of shocks (e.g., Hollenbach and McKee 1989; Draine, Roberge, and Dalgarno 1983) suggests that [O I] line emission is produced in either fast ($v_s > 50$ km s^{-1}) dissociative shocks or in slow ($v_s \leq 10$ km s^{-1}) nondissociative shocks, whereas moderate-speed, nondissociative ($v_s \sim 40$ km s^{-1}) shocks will emit primarily in the vibration-rotation transitions of H_2 and high-J rotational transitions of CO and H_2O. Thus, the observations provide an important new diagnostic for constraining models of the shocks in IC 443. We have therefore produced an extensive set of shock models to compare with our data, in order to better understand the shock physics in IC 443.

II. OBSERVATIONS

The observations were carried out from 1985–1987 with the 91 cm telescope of the Kuiper Airborne Observatory (KAO), using the facility cooled grating spectrometer (CGS) described by Erickson *et al.* (1984, 1985). The far-infrared lines of [Si II] $^2P_{3/2} \rightarrow {}^2P_{1/2}$ at 34.816 μm, [O I] $^3P_1 \rightarrow {}^3P_2$ at 63.1837 μm, and CO ($J = 22$–21) at 118.581 μm were observed in the SNR IC 443. In 1985 February [O I] and CO were observed through a 47″ aperture at two locations (see Table 1). In 1986 January [O I] was measured at seven positions through a 33″ aperture, along strip scans N-S and E-W, centered on the peak of the molecular hydrogen emission at R.A.(1950) = $6^h14^m41^s.6$, decl.(1950) = +22°22′42″ (Burton *et al.* 1988). In 1987 January an upper limit to the [Si II] emission was obtained at the [O I] peak through a 34″ aperture. At an assumed distance of 1.5 kpc for IC 443 (e.g., Georgelin 1975), 33″ corresponds to 0.25 pc.

The infrared boresight established on the ground was verified in flight to ±5″, assuming the far-infrared continuum peaks at the Kleinmann-Low Nebula (KL) (R.A.[1950] = $5^h32^m46^s.7$, decl.[1950] = −5°24′27″; Werner 1982, Thronson *et al.* 1986). Absolute positions were then determined to ±5″ by offsetting from a nearby guide star. IC 443 is extended (see Fig. 1) relative to the 4′ chopper amplitudes employed. The mean chopper orientation (measured counterclockwise from north) was 153° in 1985, 87° in 1986, and 99° in 1987. The latter two are approximately E-W, and the chopper amplitude was sufficient to ensure both reference beams were off the molecular hydrogen contours (see next section). When corrected for the difference in aperture size, the agreement between the [O I] fluxes measured in 1985 and 1986 suggests that the chopper orientation is not important.

In 1985 the focal plane was configured with six Ge:Ga detectors and afterward with 13 Ge:Be (<50 μm) and 13 Ge:Sb (>50 μm) detectors. The system noise equivalent power (NEP), including atmospheric and instrumental losses, was detemined to be 3, 1–2, and 3×10^{-14} W Hz$^{-1/2}$ at 34, 63, and 119 μm, respectively. The detector separation was ~60 km s^{-1} at all three wavelengths. The instrumental resolution was ~110 km s^{-1} for the larger aperture (1985) measurements and ~80 km s^{-1} for the smaller aperture (1986–1987) measurements. In all cases, the total bandpass of the detectors was sufficient to include the line and the adjacent continuum using a single grating position. Sequences of four 10 s integrations were taken with the source placed alternatively in right and left

TABLE 1

[O I] 63 μm LINE FLUXES IN IC 443

OFFSET		LINE FLUX (10^{-11} ergs		INTEGRATION TIME
R.A.	Decl.	s^{-1} cm^{-2})	APERTURE	(s)
0″.....	60″	0.8 ± 0.3	33″	240
0.....	30	3.1 ± 0.4	33	440
0.....	0	5.9 ± 0.5	33	160
0.....	−30	2.9 ± 0.3	33	240
0.....	−60	0.5 ± 0.3	33	320
−33.....	0	4.1 ± 0.6	33	240
33.....	0	1.3 ± 0.4	33	240
6.....	8	12.1 ± 0.6	47	200
+65.....	68	4.8 ± 0.2	47	280

NOTE.—Offsets are from the position $6^h14^m41^s.6$, +22°22′42″ (1950.0). The observations through a 33″ (FWHM) aperture were made in 1986 January, and those through a 47″ aperture were made in 1985 February.

beam. The total integration time for each observation is listed in Table 1.

The relative detector response was removed and the absolute flux calibration was achieved by dividing each measured spectrum by a spectrum of KL at a nearby continuum wavelength and then multiplying by the known flux of KL (Erickson *et al.* 1981). The aperture sizes quoted in Table 1 were measured in the laboratory by scanning a small (4″) source across the entrance aperture. The profiles are steeper than Gaussians; the effective diameter of the beam for a uniform intensity source is ~1.04 times the FWHM. The KL continuum fluxes (50″ beam) were corrected for the differences in the beam size using CGS observations at 63 μm in several different apertures. Calibration spectra on KL taken ~3 hr apart agreed to ±5%–8%. Differences in the instrumental efficiency function at nearby wavelengths were generally small and were removed using ratios of calibration spectra taken in the laboratory after the flights. The relative effects of diffraction in the telescope were estimated to be less than 7% and hence were ignored.

The [O I] line lies on the shoulder of a strongly saturated telluric water line. In 1985 the water vapor burden was determined to be 12 precipitable microns by observing several water lines in absorption against the KL and Venus continua on earlier flights in the same series. Since KL and IC 443 were observed at similar elevation angles, their water vapor burdens were assumed equal, and a correction was applied to account for the differential absorption due to the small-wavelength shifts required to avoid the [O I] line emission in Orion-KL. Similarly, the water vapor burden toward KL was measured to be 7 precipitable microns in 1986, and a correction was applied based on the wavelength and elevation differences between the two sources. The [Si II] bandpass has no telluric absorption features greater than 2%, and consequently no correction was applied to the 1987 data. The CO bandpass is devoid of significant water absorption but has a weak ozone feature several detector elements longward of the CO line wavelength. A correction of ~12% was applied to this end of the spectrum. The overall uncertainty in the absolute flux calibrations is estimated to be ±15% at 34 and 119 μm and ±25% at 63 μm.

The wavelength calibration was accomplished using laboratory measurements of water lines. The absolute wavelength calibration is good to ±30 km s^{-1}; relative shifts of ~½ this value may be significant.

III. RESULTS

a) 63 μm [O I] Line Emission

The spectra for the [O I] line at the positions observed in 1986 January are presented in Figure 2 together with least-squares Gaussian fits to them. There are four free parameters for the fits: the line strength, width, wavelength, and continuum strength. No significant continuum was detected at any of the three wavelengths observed, which is consistent with the flux levels observed by *IRAS*. The integrated line intensities are in Table 1. The maximum intensity was observed at the position of the H_2 line emission peak. The line flux is 5.9×10^{-11} ergs s^{-1} cm^{-2} in a 33″ beam. The 1985 February measurement, with a larger beam, gives the same surface brightness to within a few percent. The minimum column density of neutral oxygen in the excited $^3P_1$ state at this position is $1.3 \times 10^{+16}$ cm^{-2}, for optically thin emission, as is appropriate in most relevant shock models. Integrating over the entire observed

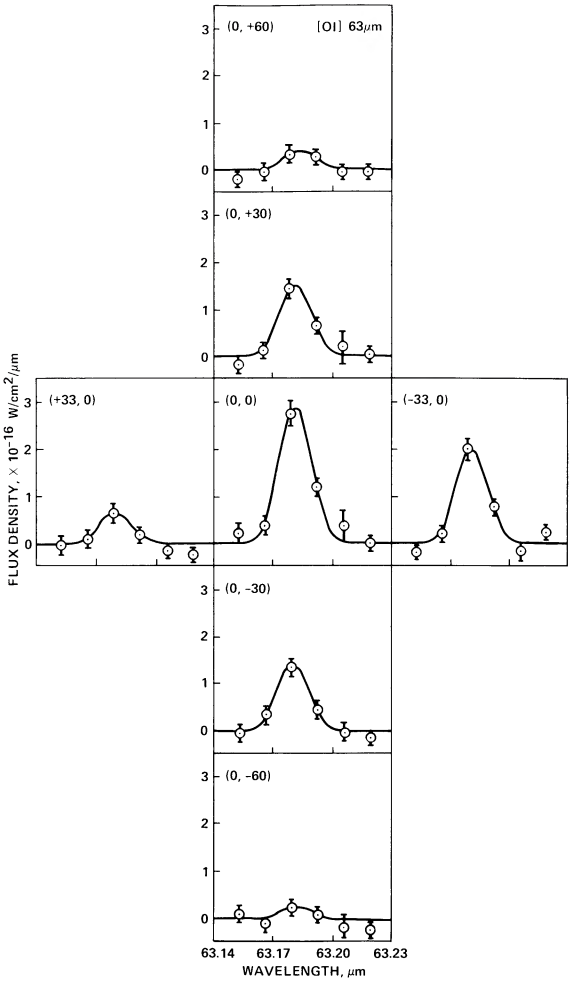

FIG. 2.—Spectra of the [O I] 63 μm lines at seven positions in IC 443, observed with a 33″ beam. The offsets are from a (0, 0) position of R.A.(1950) = 6^{h}14^{m}41^s.6, decl.(1950) = +22°22′42″. The least-squares Gaussian fits to the data are also shown.

area, the total flux is 2.3×10^{-10} ergs s^{-1} cm^{-2}, which corresponds to an [O I] luminosity of ~17 $L_\odot$ for an assumed distance to the source of 1.5 kpc. This gives a mass of neutral oxygen in the $^3P_1$ level of 3.0×10^{-4} $M_\odot$. These estimates do not allow for extinction (presumed to be negligible at 63 μm) and only apply to the small fraction of the source observed. Hence they represent lower limits on the total luminosity and mass of warm neutral oxygen in the source.

The distribution of the [O I] line emission appears similar to that of the H_2 1–0 $S(1)$ line. Figures 3*a* and 3*c* present cuts showing the relative integrated intensities of the [O I] and $S(1)$ lines (the later from Burton *et al.* 1988), in scans N-S and E-W through the emission peak. It is clear that the emission from both lines is extended relative to the beam, and that the profiles (i.e., the spatial variation in the line peaks) are similar. In order to account for the effects of different beam sizes, the H_2 data has been smoothed with a Gaussian filter of FWHM 33″. They are replotted in Figures 3*b* and 3*d*, along with a Gaussian of FWHM = 33″. The H_2 and [O I] profiles are now seen to be almost identical.

Furthermore, at the isolated position (+65″, +68″), the relative [O I] and $S(1)$ line fluxes measured are roughly the same as

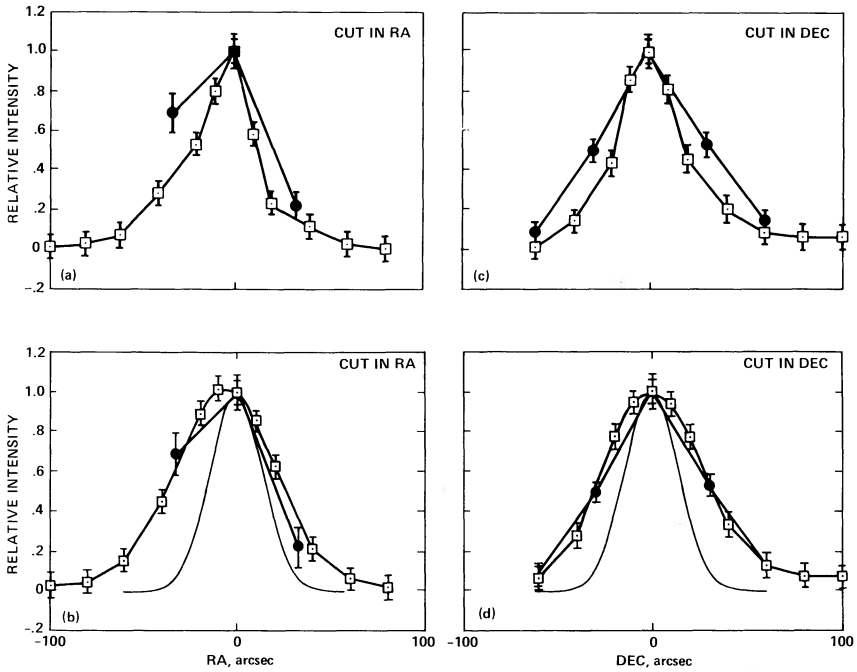

FIG. 3.—(*a*) and (*c*): Cuts in right ascension and declination through the position of peak [O I] and *S*(1) line emission showing the relative line fluxes of the [O I] line (*filled circles*) and the *S*(1) line (*open squares*). The [O I] line was measured through a 33″ beam, and the *S*(1) line was measured through a 19″ beam. (*b*) and (*d*): Same as in (*a*) and (*c*), except that the *S*(1) line flux has been smoothed with a Gaussian filter of FWHM = 33″. A Gaussian of FWHM = 33″ is also shown.

at the emission peak: the [O I] line flux is 40% of the peak [O I] value, while the *S*(1) line flux is ~30% of the peak *S*(1) value.

The mean velocity shift for the seven point map is $V_{lsr} = -15 \pm 30$ km s^{-1}. No significant shifts (to within ± 12 km s^{-1}) in the relative velocity of the [O I] line emission are seen at the positions observed. For comparison, the other shocked species observed here have broad lines with typical emission velocities extending from $V_{lsr} \sim -15$ to -60 km s^{-1}.

Though limited, these data on the [O I] line emission suggest, therefore, that its distribution is similar to that of the hot H_2. The overall morphological similarity of the H_2 emission with that from high-velocity molecules (e.g., CO, HCO^+, HCN), and from high-velocity atomic gas (21 cm H I), implies that the [O I] line has a similar distribution to all the accelerated species. We note also that the distribution of the *IRAS* 60 μm band and H_2 line emission are similar (see Fig. 1), suggesting the possibility that shocked line emission may contribute to the *IRAS* 60 μm band.

We have mapped only a tiny fraction of the shocked region of the SNR seen, for example, in H_2 1–0 *S*(1) or by *IRAS* (see Fig. 1). We will estimate the contribution of the O I to the 63 μm *IRAS* flux in these ways:

i) By assuming that the [O I] 63 μm line is proportional to the H_2 1–0 *S*(1) line over the entire source, we can crudely estimate the total [O I] emission. We estimate that the *S*(1) line flux, if observed through a 33″ beam, would be 7.0×10^{-12} ergs s^{-1} cm^{-2} at the peak position. Hence the [O I]/*S*(1) ratio is ~8.4. The total *S*(1) line luminosity is ~21 $L_\odot$ in IC 443 (Burton *et al.* 1988; Burton 1988), yielding a [O I] 63 μm line luminosity of ~180 $L_\odot$ for the entire SNR. Braun and Strom (1986*b*) and Mufson *et al.* (1986) present maps of the infrared emission from IC 443 in the *IRAS* bands. Their maps at 60 and 100 μm look similar to the H_2 1–0 *S*(1) and H I 21 cm maps; the emission comes from bright peaks distributed along an incomplete ring lying between the optical lobes of the source. Both sets of authors argue that the far-IR emission is dominated by blackbody radiation from hot, collisionally heated dust. The total emission in the 60 μm band is ~2500 $L_\odot$, and in the 100 μm band it is ~1200 $L_\odot$. Our estimate for the global [O I] emission suggests, therefore, that it accounts for ~7% of the total *IRAS* 60 μm band emission from the entire (~1°) region of IC 443. The total *IRAS* flux includes emission from parts of the source unrelated to the shocked molecular emission (e.g., from the optical lobes), so that this global estimate is a lower limit to the contribution of the [O I] emission found in directions toward shock peaks.

ii) Alternatively, we can try to compare the O I flux with the *IRAS* flux measured in the direction of the [O I] peak. Since the beam sizes are quite different (33″ for O I and an effective 6.′9 × 4.′6 for the *IRAS* measurement), we instead compare the observed H_2 1–0 *S*(1) line flux in the *IRAS* beam to the *IRAS* flux and assume the [O I] 63 μm line emission is proportional to the H_2 1–0 *S*(1) line emission, as argued above. Compared with the global estimate above, this measurement involves an extrapolation of our observed [O I]/*S*(1) correlation over a much smaller spatial extent and is, therefore, a better indicator of the contribution of [O I] to the *IRAS* flux in the direction of the shocked regions. We estimate that the H_2 1–0 *S*(1) line flux through a 6.′9 × 4.′6 beam centered on the peak is $\sim 8.4 \times 10^{-11}$ ergs s^{-1} cm^{-2}. Assuming that [O I]/1–0 *S*(1) ~8.4, we obtain for the [O I] 63 μm line flux 7.1×10^{-10} ergs s^{-1} cm^{-2}. The corresponding 60 μm band *IRAS* flux is 1.7×10^{-9} ergs s^{-1} cm^{-2} (Braun and Strom 1986). Thus the [O I] 63 μm line emission accounts for ~40% of the *IRAS* 60 μm band emission in the *IRAS* beam centered on the peak of the H_2 line emission.

iii) Using the analysis of the *IRAS* data from Mufson *et al.*

TABLE 2

ESTIMATES OF THE [O I] 63 μm LINE CONTRIBUTION TO THE FAR-IR LINE EMISSION

Parameter	Beam Size	Source	Value
A. [O I] 63 μm Line Luminosity and its Minimum Contribution to the *IRAS* 60 μm Band			
[O I] line flux	33″ aperture	Measured	5.9×10^{-11} ergs s^{-1} cm^{-2}
1–0 *S*(1) line flux	19″ aperture	Measured	3.1×10^{-12} ergs s^{-1} cm^{-2}
1–0 *S*(1) line flux	33″ aperture	Summed from 19″ map	7.0×10^{-12} ergs s^{-1} cm^{-2}
∴ [O I]/*S*(1)			8.4
1–0 *S*(1) line luminosity	Whole source	Summed from 19″ map	21 $L_\odot$
[O I] line luminosity	Whole source	Extrapolated	180 $L_\odot$
60 μm *IRAS* luminosity	Whole source	Measured	2500 $L_\odot$
∴ [O I] line contribution to 60 μm band flux	Whole source	...	7%
B. [O I] 63 μm Contribution to 60 μm *IRAS* Flux at Shock Peak (Braun and Strom 1986*b*)			
1–0 *S*(1) line flux	6.9 × 4.6	Summed from 19″ map	8.4×10^{-11} ergs s^{-1} cm^{-2}
[O I]/*S*(1)	...	From A	8.4
[O I] line flux	6.9 × 4.6	Extrapolated	7.1×10^{-10} ergs s^{-1} cm^{-2}
60 μm *IRAS* flux	6.9 × 4.6	Measured	1.7×10^{-9} ergs s^{-1} cm^{-2}
∴ [O I] line contribution to 60 μm band flux	6.9 × 4.6	Shock Peak	40%
C. [O I] 63 μm Contribution to 60 μm *IRAS* Flux at Shock Peak (Mufson *et al.* 1986)			
1–0 *S*(1) line flux	4.3 × 1.9	Summed from 19″ map	4.6×10^{-11} ergs s^{-1} cm^{-2}
[O I]/*S*(1)	...	From A	8.4
[O I] line flux	4.3 × 1.9	Extrapolated	3.9×10^{-10} ergs s^{-1} cm^{-2}
60 μm *IRAS* flux	4.3 × 1.9	Measured	5.2×10^{-10} ergs s^{-1} cm^{-2}
∴ [O I] line contribution to 60 μm band flux	4.3 × 1.9	Shock Peak	75%

(1986) (and McCollough, private communication), the 60 μm flux in a 4.3 × 1.9 beam centered on the H_2 emission peak is 5.2×10^{-10} ergs s^{-1} cm^{-2}. We estimate an *S*(1) line flux in this beam of 4.6×10^{-11} ergs s^{-1} cm^{-2}, from which we obtain an [O I] line flux of 3.9×10^{-10} ergs s^{-1} cm^{-2}. Hence for these data, which are confined to an even smaller region around the peak of H_2 line emission, the [O I] 63 μm line contribution to the 60 μm band flux is 75%.

These estimates are summarized in Table 2. They are, of necessity, crude, but they clearly indicate that [O I] 63 μm line emission is an important contributor to the far-infrared emission from IC 443. The morphological similarity of the H_2 and *IRAS* 60 μm maps therefore strengthens our earlier conclusion that the distribution of the hot O I and shocked H_2 emitting gas are similar. More extended observations of [O I] 63 μm are planned which should improve the accuracy of these estimates.

b) *118 μm CO (J = 22–21) Upper Limit*

We searched for the $J = 22$–21 CO line at 118.6 μm with a 47″ beam at two locations but failed to detect it. The 3 σ upper limits on the line strength are $\leq 1.0 \times 10^{-11}$ ergs s^{-1} cm^{-2} at (6″, 8″) and $\leq 1.2 \times 10^{-11}$ ergs s^{-1} cm^{-2} at (65″, 68″) (positions with respect to the [O I] peak position given above). The integration times were 600 and 400 s, respectively. The spectra are shown in Figure 4.

c) *34 μm [Si II] Line Upper Limit*

We searched for the [Si II] $^2P_{3/2} \rightarrow {}^2P_{1/2}$ at 34.8 μm with a 34″ beam at the [O I] line emission peak but failed to detect it. The 3 σ upper limit on the line strength, obtained in 2400 s of integration time, is $\leq 6 \times 10^{-12}$ ergs s^{-1} cm^{-2}. The spectrum is shown in Figure 5.

IV. FAR-ULTRAVIOLET OR X-RAY EXCITATION MECHANISMS

In this section we discuss two possible excitation mechanisms for the [O I] line emission, X-rays and far-UV radiation, and we conclude that they cannot explain the emission.

a) *Photodissociation Region Model of IC 443*

Photodissociation regions (PDRs, see Tielens and Hollenbach 1985) are dense neutral clouds illuminated by UV photons. The gas in PDRs is heated by the photoelectric ejection of superthermal electrons from the surfaces of grains. We conclude that the bulk of the [O I] emission in IC 443 is not from PDR because: (1) there is no H II region near to the emitting gas which would indicate the presence of illuminating UV photons to excite the gas, and (2) due to the low efficiency of photoelectric heating, the [O I] 63 μm luminosity is, on theoretical grounds, always less than ~4% of the far-infrared continuum luminosity L_{IR} and, observationally, it is always less than about 1% of L_{IR} in PDRs. The 17 $L_\odot$ of [O I] 63 μm measured in the small region observed is much greater than 4% of the L_{IR} from this region (which is less than 120 $L_\odot$, Braun and Strom 1986*b*).

b) *X-Ray Heating of Molecular Cloud*

Another possibility is that X-rays from the hot supernova remnant interior are absorbed by the molecular gas and heat and dissociate the gas to provide the observed emission. Draine and Woods (1989) have analyzed the effect of X-rays in molecular gas and conclude that significant H_2, [O I] 63 μm, and [C II] 158 μm emission can be produced.

However, here we tentatively rule out X-ray heating of the H_2 and O I on energetic grounds. The total X-ray luminosity from IC 443, over the energy range 0.5–4.5 keV and an angular

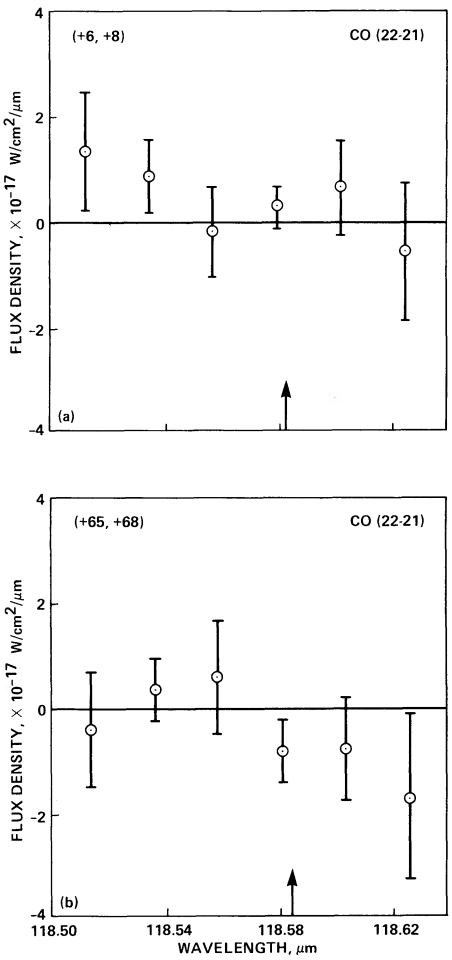

FIG. 4.—Spectra taken at the (Doppler corrected) wavelength of the CO $J = 22$–21 line at two positions in IC 443, showing no detection of the line. The central wavelength expected for the line is shown by the arrow. The positions are with respect to the same (0, 0) as for the [O I] observations.

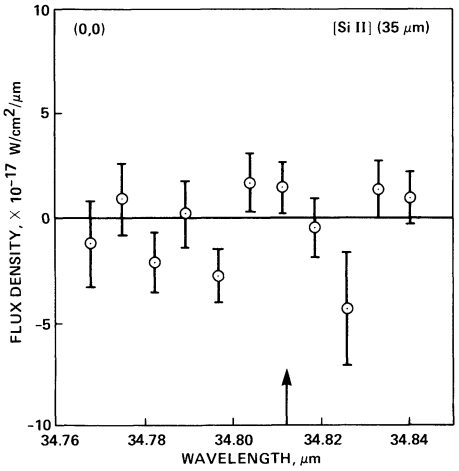

FIG. 5.—Spectrum taken at the wavelength of the [Si II] line at the position of peak [O I] line emission in IC 443, showing no detection of the line. The central (Doppler corrected) wavelength expected for the line is shown by the arrow.

extent of $\sim 1°$, has been calculated to be 40 $L_\odot$ (Watson *et al.* 1983, correcting their estimate to a source distance of 1.5 kpc). This is twice the [O I] luminosity from the small region measured and less than the ~ 180 $L_\odot$ estimated for the total [O I] luminosity of the source. In addition, the total H_2 luminosity, corrected for 1 mag of extinction at 2 μm, is of order 1000 $L_\odot$. Finally, we note that the [O I] 63 μm and H_2 2 μm emission regions subtend a small solid angle relative to the X-ray emitting interior of the supernova remnant, intercepting only a small percentage ($\sim 5\%$) of the X-ray luminosity. Therefore, only a small fraction of the 40 $L_\odot$ of intrinsic X-ray luminosity can be absorbed in the infrared emitting region. We conclude that X-ray heating can only be significant in producing the [O I] 63 μm or H_2 2 μm if the intrinsic luminosity has been underestimated by a factor of at least 10^2–10^3.

V. MOLECULAR SHOCK MODELING OF IC 443

In this section we conclude that the IR line emission from IC 443 is shock-excited and attempt to model it. We first discuss the evidence which indicates that the emission is shock-excited, provide some general constraints which must apply to any model for the emission, and then describe the models. The results have implications for our theoretical understanding of shock physics, and we finish by outlining future observations which may provide answers to some of the questions raised.

a) General Considerations

The [O I] line emission spatially correlates with the H_2 1–0 $S(1)$ line emission, which is likely to be shock-excited (Burton *et al.* 1988), and with other high-velocity molecules (e.g., CO) and high-velocity atomic gas (21 cm H I emission), which are believed to be shock accelerated (e.g., White *et al.* 1987; Braun and Strom 1986*a*). We feel that the morphology of the [O I] emission is strong evidence for its shock origin and endeavor to find an appropriate shock model for the emission.

There are three basic observational constraints which we impose on any shock model: (*a*) a relatively uniform and constant driving pressure, (*b*) fairly constant [O I] 63 μm/H_2 1–0 $S(1)$ and H_2 1–0 $S(1)$/2–1 $S(1)$ line ratios over the entire source, and (*c*) the observed line fluxes at the peak. We consider each of these in turn:

1) *Driving pressure.*—The SN blast wave in IC 443 has propagated outward, forming a bubble as it interacts with various components of the interstellar medium. The hot X-ray emitting gas filling the interior of the bubble keeps the expansion in approximate pressure equilibrium, so the pressure driving shock waves through various density clouds or clumps is approximately constant. Using derived values of the gas density, temperature, and shock velocity obtained through observations of atomic and molecular lines, X-rays, and far-infrared emission, we can estimate the ram pressure, $n_0 v_s^2$ (where n_0 is the preshock hydrogen density), of the shocks in the various emitting regions of the source. These are listed in Table 3. X-ray observations provide a lower limit of $p \equiv n_0 v_s^2 > 10^5$ cm^{-3} (km s^{-1})^2, whereas the nondetection of Brγ provides an upper limit of $p < 5 \times 10^7$ cm^{-3} (km s^{-1})^2 (note the use of unconventional pressure units). Optical lines, CO, H I, and *IRAS* observations all give ram pressures of order 10^5–10^6 cm^{-3} (km s^{-1})^2, with large uncertainties. Thus, we shall attempt to model the line emission at the H_2 emission peak in IC 443 as arising from shocks driven by a ram pressure of $\sim 10^5$–10^7 cm^{-3} (km s^{-1})^2.

TABLE 3

SHOCK RAM PRESSURES IN IC 443

Observation	Derived Parameters	Ram Pressure $n_0 v_s^2$ cm^{-3} (km s^{-1})^2	Reference
X-rays 0.5–1.5 keV	$T = 10$ [6–28] $\times 10^6$ K, $n_0 = 0.3$ [0.1–0.6] cm^{-3}, $v_s = 800$ km s^{-1}	>20 [6–40] $\times 10^4$	1
X-rays 1.1–7.5 keV	$T = 2 \times 10^7$ K, $n_e \geq 0.2$ cm^{-3}	$>6 \times 10^4$	2
X-rays 2–10 keV	$T = 1.2 \times 10^7$ K, $n_0 = 0.8$ cm^{-3}	$>4 \times 10^4$	3
Optical Filaments ..... ([O III], [N II], [S II])	$n_0 = 10$–20 cm^{-3} $v_s = 65$–100 km s^{-1}	4–20 $\times 10^4$	4
CO ($J = 1$–0)	$v_s \geq 15$–50 km s^{-1}, Assume $n_0 = 3000$ cm^{-3}	≥ 3–40×10^5	5
H I 21 cm	$n_0 = 10^4$ and 420 cm^{-3}, $v_s \geq 15$ and 75 km s^{-1}	$\geq 2 \times 10^6$	6
Brγ	$n_0 < 5 \times 10^3$ cm^{-3}, Assume $v_s \sim 100$ km s^{-1}	$<5 \times 10^7$	7
H51α	$n_0 < 5 \times 10^3$ cm^{-3}, Assume $v_s \sim 100$ km s^{-1}	$<5 \times 10^7$	8

NOTES.—The derived parameters are those listed by the authors; n_0 is the preshock gas hydrogen number density, v_s is the shock velocity, T is the gas temperature, and n_e is the electron density. Lower limits for X-ray pressures assume filling factor $f = 1$; for $f < 1$, density increases. For CO and H I lines, the velocities are line-of-sight velocities and thus provide a lower limit on the ram pressure. Brγ and H51α provide upper limits based on upper limits to the line fluxes.

REFERENCES.—(1) Malina *et al.* 1976; (2) Watson *et al.* 1983; (3) Petre *et al.* 1988; (4) Fesen and Kirshner 1980; (5) White *et al.* 1987; (6) Braun and Strom 1986*a*; (7) Burton *et al.* 1988; (8) Burton *et al.* 1990, McKee and Hollenbach 1987.

2) *Line ratios.*—The good correlation of [O I] with the H_2 1–0 $S(1)$ suggests that the emission arises in the same shocks and that the intensity peaks correspond to peaks in the beam filling factor. In addition, the data suggest that we require the [O I]/H_2 1–0 $S(1)$ line ratio from shocks of similar ram pressure to be fairly constant. In other words, the line ratio should be robust and should not require a fine-tuning of the n_0 and v_s combination. The H_2 1–0 $S(1)$/2–1 $S(1)$ line ratio has been measured at several locations in the source (Burton *et al.* 1988) and found to be ~ 10 at each position. Thus we also require this line ratio to be robust in any model for the emission.

3) *Line fluxes.*—Table 4 is a compilation of the fluxes of shocked molecular and atomic lines, shock-accelerated lines, and IRAS 60 and 100 μm band emission, observed at the peak. Specific intensities are listed in Table 6. The H_2 line intensities depend on the extinction in the near-infrared. Burton *et al.* (1988) estimate the extinction to be similar to that toward the shocked gas in BN-KL, or ~ 1 mag (Brand *et al.* 1988). Since this estimate is quite uncertain, we assume that the extinction at 2.1 μm is 0–2 mag and the extinction at 3.8 μm is 0–1 mag (see Table 6).

b) *Detailed Shock Models*

We have attempted to model the line fluxes in Table 4 using jump shock (J shock) and continuous shock (C shock) models. In a J-type shock (e.g., Kwan 1977; London, McCray, and Chu 1977; Hollenbach and Shull 1977; Hollenbach and McKee 1989), there is an abrupt transition layer where the hydrodynamic variables (velocity, density, temperature) change discontinuously in a "jump," with negligible thickness. All the gas heating occurs within this jump region, negligible cooling emerges from the region, and the temperature rises suddenly. The gas subsequently cools in a hot postshock relaxation region through the processes of line emission and molecule dissociation. In contrast, for a C-type shock (e.g., Draine 1980), the hydrodynamic variables vary "continuously" from preshock to postshock values. Heating occurs by friction between ions and neutrals in a drag region *which has a length comparable with the cooling length.* Heating and cooling processes compete, and a different picture of the emission region than from a J-type shock emerges. The temperature gradually increases to a relatively low maximum, and then drops. C shocks are nondissociative shocks in molecular gas of relatively low ionization. J shocks are either dissociative or require gas of relatively high ionization (see Hollenbach, Chernoff, and McKee 1989).

The models run are one-dimensional, hydrodynamic, steady state codes, which determine the energy balance self-consistently at each point in the shock and follow the gas phase chemistry. Specific details concerning them can be found in Hollenbach and McKee (1989) for the J shock models and in Chernoff, Hollenbach, and McKee (1982) and Draine, Roberge, and Dalgarno (1983) for the C shock models. Here we only summarize the pertinent results. The basic conclusion, despite considering an extensive parameter space, is that we find it extremely difficult to fit both the [O I] and the H_2 with a single shock model.

Seven representative classes are considered, involving four basic types of shock waves, that reflect different physical conditions which may be present: (*a*) fast dissociative J shocks ($v_s \geq 30$ km s^{-1}) (class A), (*b*) slow nondissociative or particularly dissociative J shocks ($v_s \leq 25$ km s^{-1}) (classes B and C), (*c*) slow C shocks with low peak temperatures ($T \leq 300$ K) so that neutral-neutral reactions with activation energies are suppressed ($v_s \leq 15$ km s^{-1}) (class D), and (*d*) moderate to fast C shocks with peak temperatures $T \sim 1000$–3000 K, near the

TABLE 4

SHOCKED LINE AND BROAD-BAND INTENSITIES FOR IC 443

A. SHOCK-HEATED LINE EMISSION

Line	Wavelength (μm)	Beam Size	Flux (ergs s^{-1} cm^{-2})	Reference
H_2 1–0 $S(1)$	2.12181	19″	$3.1 \pm 0.1\ (-12)$	1
Brγ	2.1655	19	$\leq 8.\ (-14)$	1
H_2 2–1 $S(1)$	2.2477	19	$2.4 \pm 0.5\ (-13)$	1
H_2 0–0 $S(13)$	3.846	5	$9.8 \pm 0.8\ (-14)$	2
[Si II] $^2P_{3/2} \rightarrow {}^2P_{1/2}$	34.815	34	$\leq 6.\ (-12)$	3
[O I] $^3P_1 \rightarrow {}^3P_2$	63.1837	33	$5.9 \pm 0.5\ (-11)$	3
CO $J = 22$–21	118.581	47	$\leq 1.\ (-11)$	3
H51α	6225.7	38	$\leq 2.\ (-17)$	4

B. SHOCK-ACCELERATED LINE EMISSION

Line	Wavelength (μm)	Beam Size	Flux (ergs s^{-1} cm^{-2})	Reference
CO $J = 1$–0	2.6008	16″	$9.2 \pm 0.1\ (-16)$	4
$C^{13}O$ $J = 1$–0	2.7204	16	$\leq 2.\ (-17)$	4
CS $J = 2$–1	3.0597	19	$1.3 \pm 0.3\ (-17)$	4
HCO_+ $J = 1$–0	3.3613	19	$3.3 \pm 0.1\ (-16)$	4
HCN $J = 1$–0	3.3824	19	$9.8 \pm 1\ (-17)$	4
CS $J = 1$–0	6.1193	38	$9 \pm 6\ (-18)$	4
H I	210.	21″ × 56″	$N_{HI} = 1.7\ (+21)$ cm^{-2}	5

C. BROAD-BAND FAR INFRARED EMISSION

Line	Wavelength (μm)	Beam Size	Flux (ergs s^{-1} cm^{-2})	Reference
IRAS 60 μm	44–76	6.9 × 4.6	$1.7\ (-9)$	6
IRAS 100 μm	84–116	6.9 × 4.6	$9.1\ (-10)$	6
IRAS 60 μm	44–76	4.3 × 1.9	$5.2\ (-10)$	7
IRAS 100 μm	84–116	7.5 × 5.7	$1.8\ (-9)$	7

NOTES.—The position when the lines were measured is $6^h14^m41^s.7 \pm 0^s.1$, $+22°22'40 \pm 2''$ (1950.0). Upper limits quoted are 3 σ. For CO $J = 1$–0, the velocity range is -80 km s^{-1} to -4 km s^{-1}, for H I 21 cm it is -43 km s^{-1} to -18 km s^{-1}. For other lines, the entire velocity range of emission is included in the line fluxes.

REFERENCES.—(1) Burton *et al.* 1988; (2) Burton *et al.* (1989*a*); (3) This paper; (4) Burton *et al.* 1990; (5) Braun and Strom 1986*a*; (6) Braun and Strom 1986*b*; (7) Mufson *et al.* 1986, McCollough, private communication.

dissociation limit for H_2 ($v_s \sim 25$–40 km s^{-1}) (classes E, F, and G). Class C differs from class B, and class F differs from class E, only in that the oxygen chemistry is suppressed so that the oxygen which is not locked up in CO remains in atomic form. Class G is a higher pressure model ($\sim 6 \times 10^8$ cm^{-3} [km s^{-1}]^2) from Draine, Roberge, and Dalgarno (1983), which violates the pressure constraint, but it was included because it produces a reasonable fit to the H_2 1–0 $S(1)$ and [O I] 63 μm line intensities.

Table 5 presents the "best-fit" models (i.e., closest to the observed fluxes) in each of the seven classes (model A refers to the "best" model in class A, etc.). In reaching these fits, over 50 new models were run, in the ram pressure range 10^6–10^7 cm^{-3} (km s^{-1})^2, and in the velocity ranges given below for each model. Previously published models allowed us to restrict the range of parameter space explored in order to produce a manageable number of models and concentrate on the most promising classes. We found, in fact, that ram pressures below 10^7 cm^{-3} (km s^{-1})^2 produce too little absolute intensity in the [O I] and H_2 2 μm lines, so that all the models listed have pressures near the upper limit. We have implicitly assumed that the area filling factor of shocks within the beam is of order unity. If the shocks are limb-brightened, or if the region is sufficiently clumped that there are many shocks along a line of sight, so that the area filling factor is $\gg 1$, then the ram pressure can be lowered somewhat. All models assume the following chemical composition of the *preshock* gas: all H in H_2, all C in CO, all O in O I except that in CO, and elemental oxygen abundance greater than carbon. We note, however, that chemistry is included in the models so that the postshock composition is calculated self-consistently. The gas phase abundance of the elements can be derived from the gas phase depletion factors, ∂, given in Table 5. Also listed are the preshock magnetic field component normal to v_s and the preshock ionization fraction; J shocks are quite insensitive to these parameters, and C shocks are insensitive to the ionization fraction if $x_i < 6 \times 10^{-7}$ (see, for example, Hollenbach 1982).

Table 6 compares the observed intensities with the theoretical predictions for the best fit in each of the classes of shock models. We discuss these in turn below.

i) *Class A: Fast Dissociative Jump Shocks*

Model A represents a best-fit in the velocity range 30 km $s^{-1} < v_s < 150$ km s^{-1}. Dissociative J shocks are strong in [O I] 63 μm, and the shock was chosen to fit this line. However, model A predicts weak H_2 1–0 $S(1)$ and 2–1 $S(1)$ lines. In addition, the 1–0/2–1 $S(1)$ line ratio is too small, resulting from the formation pumping of reforming postshock molecules. Since the shock produces extensive ionization, the Brγ and [Si II] 35 μm lines are strong and marginally exceed the observed upper limits. The most serious discrepancy, though, is that a fast J shock which provides sufficient [O I] line emission also produces copious optical and UV emission. This short-wavelength emission is absorbed by the dust (recall

TABLE 5

SHOCK MODELS

SHOCK PARAMETERS	MODEL A[a]	B[b]	C[b]	D[c]	E[c]	F[c]	G[d]
Type	"Fast" *J*	"Slow" *J*	"Slow" *J*	"Slow" *C*	"Fast" *C*	"Fast" *C*	"Fast" *C*
Speed (km s^{-1})	100	10	10	10	40	40	25
Preshock Density (cm^{-3})	10^3	10^5	10^5	10^5	10^4	10^4	10^6
Pressure (cm^{-3} [km s^{-1}]^2)	10^7	10^7	10^7	10^7	1.6×10^7	1.6×10^7	6.3×10^8
$B_{0\perp}$[e] (μG)	10	100	100	316	100	100	1000
Ionization Fraction[f]	...	...	...	$\leq 10^{-6.5}$	$\leq 10^{-6.5}$	$\leq 10^{-6.5}$	$\leq 10^{-6.5}$
Area Filling Factor	2	4	4	2	4	4	1
∂(C)	0.62	0.62	0.62	0.25	0.25	0.25	0.20
∂(O)	0.80	0.80	0.80	0.50	0.50	0.50	0.56
∂(Si)	0.10	0.10	0.10	0.03	0.03	0.03	...
∂(Fe)	0.04	0.04	0.04	0.03	0.03	0.03	...
Other	...	...	O Chemistry suppressed	...	...	O Chemistry suppressed	...

NOTES.—∂(C), ∂(O), ∂(Si), and ∂(Fe) are the depletions with respect to cosmic abundances.

[a] From Hollenbach and McKee 1989.

[b] New runs with code from Hollenbach and McKee 1989.

[c] New runs supplied by D. Chernoff from code described in Chernoff, Hollenbach, and McKee 1982.

[d] From Draine, Roberge, and Dalgarno 1983 and Draine and Roberge 1984.

[e] *J* shock spectra quite insensitive to $B_{0\perp}$.

[f] *J* shock IR spectra are not sensitive to preshock ionization.

TABLE 6

OBSERVED VERSUS MODEL LINE INTENSITIES (ergs s^{-1} cm^{-2} sr^{-1})

Line	Observed	A ("Fast J")	B ("Slow J")	C ("Slow J")	D ("Slow C")	E ("Fast C")	F ("Fast C")	G ("Fast C")
H_2 1–0 *S*(1)	3.5 (−4) −2.2 (−3)[a]	3.6 (−5)	5.3 (−4)	6.9 (−4)	<1 (−10)	3.6 (−3)	3.6 (−3)	3 (−3)
H_2 2–1 *S*(1)	2.6 (−5) −1.6 (−4)[a]	1.7 (−5)	4.3 (−5)	4.1 (−5)	<1 (−10)	3.2 (−4)	3.2 (−4)	1 (−4)
H_2 0–0 *S*(2)	...	1.0 (−6)	4.5 (−5)	1.1 (−4)	4.2 (−5)	3.8 (−3)	3.8 (−3)	2 (−3)
H_2 0–0 *S*(13)	2.7 (−5) −7.0 (−5)[a]	3.8 (−6)	1.7 (−5)	1.9 (−5)	<1 (−10)	not available		1 (−5)
H_2 Total	...	2.6 (−4)	1.0 (−2)	1.4 (−2)	6.4 (−4)	1.4 (−1)	1.4 (−1)	1.4 (−1)
CO J = 22–21	<2.5 (−4)	2.4 (−8)	1.6 (−4)	3.4 (−4)	1.7 (−8)	3.8 (−5)	3.8 (−5)	2 (−3)
CO Total	...	2.2 (−5)	3.2 (−3)	6.5 (−3)	1.2 (−3)	2.5 (−3)	2.5 (−3)	1.4 (−2)
H_2O Total	...	6.0 (−7)	1.0 (−2)	5.3 (−7)	7.2 (−4)	2.3 (−2)	<1 (−6)	1.3 (0)
OH Total	...	1.7 (−6)	1.2 (−5)	3.2 (−9)	2.6 (−6)	5.2 (−4)	<1 (−6)	4.3 (−3)
Brγ	<2.8 (−5)	4.0 (−5)	<1 (−10)	1.2 (−14)	<1 (−10)	<1 (−10)	<1 (−10)	<1 (−10)
H51α	<7.5 (−10)	3.4 (−11)	<1 (−14)	<1 (−14)	<1 (−14)	<1 (−14)	<1 (−14)	<1 (−14)
[O I] 63 μm	2.9 (−3)	3.0 (−3)	2.1 (−7)	2.9 (−3)	2.2 (−3)	8.2 (−5	~2 (−3)	3 (−3)
[O I] 145 μm	...	9.0 (−5)	6.8 (−9)	7.2 (−5)	6.8 (−4)	4.8 (−6)	~1 (−4)	1 (−4)
[C I] 370 μm	...	4.2 (−5)	1.4 (−12)	3.1 (−10)	1.4 (−4)	5.2 (−6)	5.2 (−6)	3 (−4)
[C I] 609 μm	...	7.4 (−6)	2.0 (−13)	5.2 (−11)	1.4 (−5)	6.4 (−7)	6.4 (−7)	1 (−5)
[C II] 158 μm	...	3.2 (−4)	<1 (−10)	2.9 (−10)	<1 (−10)	<1 (−10)	<1 (−10)	<1 (−10)
[Ne II] 12.8 μm	...	6.6 (−4)	<1 (−10)	<1 (−10)	<1 (−10)	<1 (−10)	<1 (−10)	<1 (−10)
[Si II] 35 μm	<2.8 (−4)	2.0 (−4)	<1 (−6)	<1 (−6)	<1 (−6)	<1 (−6)	<1 (−6)	<1 (−6)
[Fe II] 26 μm	...	1.8 (−4)	<1 (−6)	<1 (−6)	<1 (−6)	<1 (−6)	<1 (−6)	<1 (−6)
Grain 60 μm	...	1.2 (−1)[b]	4 (−4)[c]	4 (−4)[c]	...	...	...	...
Grain 100 μm	...	6 (−2)[b]	2 (−4)[c]	2 (−4)[c]	...	...	...	...
IRAS 60 μm[d]	~8 (−3)[e]	1.2(−1)	4 (−3)	4 (−3)	3 (−3)	9 (−3)	≤2 (−3)	5 (−1)
IRAS 100 μm[e]	~4 (−3)[e]	6 (−2)	3 (−3)	2 (−3)	2 (−4)	4 (−3)	8 (−4)	2 (−1)

[a] Corrected for extinction.

[b] The grain emission is calculated from $\frac{1}{2} n_0 v_s^3$.

[c] $\frac{2}{3}$ of the grain emission is assumed to be in the 60 μm band and $\frac{1}{3}$ is assumed to be in the 100 μm band. The grain temperature is 40 K in the *J* shock and 20 K in the *C* shock models.

[d] Sum of grain (60 μm) + [O I] 63 μm + H_2O (60 μm) + CO (60 μm).

[e] 10% of the emission from the *IRAS* 4.6 × 6.9 beam is assumed to originate in the [O I] 63 μm beam of 33". For the line contributions to the *IRAS* flux, it was assumed that for H_2O 37% of the total radial emission falls in the 60 μm band and 15% falls in the 100 μm band (Neufeld and Melnick 1987), while for CO 10% and 33% does.

[f] Sum of grain (100 μm) + H_2O (100 μm) + CO (100 μm).

$A_V \geq 10$ toward the observed regions) and reradiated as far-IR continuum. The grain emission in the *IRAS* 60 and 100 μm bands is given in Table 6, as well as an estimate of the fraction of the observed *IRAS* flux (beam size 6.'9 × 4.'6) which lies in the 33″ beam of the peak [O I] 63 μm observations. Note that the fast J shock produces an order of magnitude more grain continuum than was observed by *IRAS*.

ii) *Class B: Slow, Partially Dissociative Jump Shocks*

Numerous slow, nondissociative or partially dissociative J-shock models in the 5–25 km s^{-1} range were studied, and model B represents one of the best fits to the H_2 data given the pressure constraints. These shocks are very weak in [O I] 63 μm, because of the rapid conversion of atomic oxygen to OH and H_2O in the $T \geq 1000$ K gas implied by H_2 emission. The CO 22–21 emission lies very close to the observed upper limit, and the H_2O emission is intense. The CO and H_2O lines dominate the grain continuum emission in the *IRAS* 60 μm and 100 μm bands, and their predicted emission lies close to the *IRAS* observed values. It should be noted that for the magnetic field strengths and ionization fractions in molecular gas of preshock density $n_0 = 10^5$ cm^{-3}, theoretical expectations are that 10–20 km s^{-1} shocks should not be J shocks, but should be C shocks instead (e.g., see Hollenbach, Chernoff, and McKee 1989).

iii) *Class C: Slow, Partially Dissociative Jump Shocks with Oxygen Chemistry Suppressed*

Due to the difficulty in finding a suitable single shock model to fit the observations, in class C we have relaxed certain theoretical expectations in an attempt to find a good fit. In a similar vein, Brand *et al.* (1988) and Burton *et al.* (1989*b*) find that 10–20 km s^{-1} J shocks provide a better fit to the H_2 shock data in the BN-KL region of Orion than do C shock models. Our model C is very similar to the Brand *et al.* (1988) model for Orion in that it is a slow J shock which suppresses H_2O cooling. It represents the best fit of a number of J shock model runs with $v_s = 5$–25 km s^{-1} where we have forced oxygen to stay in atomic form in the cooling postshock gas. This is equivalent to suppressing the neutral-neutral reaction $O + H_2 \rightarrow OH + H$ or to hypothesizing a fast destruction mechanism for OH and H_2O molecules which *rapidly* returns oxygen to atomic form. It should be emphasized that we can offer no theoretical arguments for why this may be the case. Nevertheless, as in Orion, this type of single shock provides the best fit to all the data, and in particular can fit both the H_2 and the O I. The Brand *et al.* model, however, is a semianalytic model which does not self-consistently solve for the energy balance and chemical composition through the shock, whereas our models do.

Model C matches the H_2 and [O I] 63 μm data without violating the other observational constraints such as those on the ionized gas and the IR continuum. The CO $J = 22$–21 observational upper limit is slightly below the model C predicted emission; however, model C assumes relatively high gas phase abundance of carbon (see Table 5), and a lower carbon abundance would put the theoretical model emission below the observational constraint. Another positive feature about model C is that the intensities are relatively robust to changes in v_s for a given driving pressure. Models with velocities in the range 10–20 km s^{-1} all produce relatively good fits; although shocks in the 15–20 km s^{-1} runs produce 1–0/2–1 $S(1)$ ratios of ~ 5, which are smaller than those observed (~ 10, Burton *et al.* 1988), with only the ~ 10 km s^{-1} shocks replicating the observed ratio.

iv) *Class D: Slow Continuous Shocks*

Slow C shocks are strong in [O I] 63 μm if the preshock gas has a high O abundance but weak in the vibrational lines of H_2 (see also Draine, Roberge, and Dalgarno 1983). The peak temperatures in these shocks are too low (≤ 300 K) to enable the neutral-neutral reactions which transfer O to OH and H_2O to overcome their activation barriers. Therefore, the oxygen stays atomic and the [O I] 63 μm is intense. By the same token, however, the temperatures are too low to excite the vibrational lines of H_2, and the 1–0 $S(1)$ and 2–1 $S(1)$ line intensities lie far below the observational intensities. Model D represents a fit to the O I observations. Note that the [O I] 63 μm emission is optically thick, so that the [O I] 145 μm/63 μm ratio is much higher than for optically thin gas. Thus, a search for [O I] 145 μm may help determine whether slow C shocks contribute to the [O I] 63 μm line emission.

v) *Class E: Fast Continuous Shocks*

Fast C shocks with velocities ~ 40 km s^{-1} heat the molecular gas to ≥ 2000 K and produce strong H_2 vibrational emission but weak [O I] emission. In these shocks the neutral-neutral chemistry rapidly converts O to OH and H_2O and suppresses the [O I] 63 μm intensity. Model E represents a fit to the observed H_2 emission. However, we note that the ratio of the H_2 1–0 $S(1)$/2–1 $S(1)$ lines is sensitive to the shock velocity. In addition, the predicted CO $J = 22$–21 line emission lies somewhat above the observed upper limit (again, this could indicate a lower gas phase C, and hence CO, abundance than was used in the theoretical model). In this model, the H_2O emission can account for all the observed *IRAS* 60 μm and 100 μm band emission.

vi) *Class F: Fast Continuous Shocks with Oxygen Chemistry Suppressed*

Class F, like class C, represents an ad hoc assumption that the oxygen stays atomic in the postshock gas. There is perhaps a little more justification for this assumption here, since the emitting neutral gas is at a much lower density ($\sim 2 \times 10^4$ cm^{-3}) than the emitting gas in the J-shock ($> 10^6$ cm^{-3}). In the low-density case, the H_2 vibrational population may be extremely non–LTE, with essentially all of the H_2 in $v = 0$. The chemical reaction of H_2 ($v = 0$) with O to form OH may be quite inhibited (see Wagner and Graff 1987). We note, however, that the rates would have to be much more inhibited than suggested by these authors. Unlike model C, model F is not robust; the [O I] 63 μm to 1–0 $S(1)$ ratio is very sensitive to the shock velocity.

vii) *Class G: Intermediate-Velocity High-Pressure Continuous Shocks*

Model G represents an intermediate-velocity C shock which fits the H_2 and [O I] 63 μm intensities (taken from Draine, Roberge, and Dalgarno 1983). However, there are several observational constraints which rule out this single shock possibility. First, the expected CO $J = 22$–21 line emission from such a shock (Draine and Roberge 1984) is an order of magnitude larger than our observed upper limits. Second, the H_2O rotational emission is so intense that the fraction in the *IRAS* 60 + 100 μm bands exceeds the observed emission by a factor 10–100. Third, the required driving pressure for this shock [$\sim 6 \times 10^8$ cm^{-3} (km s^{-1})^2] exceeds the observationally determined pressures by almost two orders of magnitude.

c) Implications

In this section we draw some conclusions from our extensive shock modeling efforts for IC 443. First, considering only the

shock models which conform to our current theoretical understanding (i.e., *C* shocks for velocities below ~ 45 km s^{-1} and *J* shocks above, with "normal" oxygen chemistry), there is no single shock model which fits the data. The best fit to the peak emission is two *C* shocks with the same driving pressure [$\sim 10^7$ cm^{-3} (km s^{-1})^2] filling the beam, as specified by models D and E. The low-velocity shock provides the [O I] emission (class D) and the high-velocity shock provides the H_2 emission (class E). This two-shock picture can be regarded as representative of a distribution of shock velocities within the beam, with the faster shocks being of class E and the slower shocks of class D. The resultant line intensities are a linear combination of all the shocks within the beam. Such a composite model, however, cannot explain why the [O I] 63 μm/H_2 1–0 *S*(1) and H_2 1–0 *S*(1)/2–1 *S*(1) line ratios stay relatively constant as one maps the region. It would imply that the ratio of fast shock area to slow shock area remains constant in the beam (or, equivalently, that the distribution of shock velocities within the beam remains constant); such a requirement seems ad hoc and improbable.

Fast, dissociative *J* shocks (class A) cannot significantly contribute to the [O I] 63 μm or H_2 emission because their filling factors are constrained by the observed upper limits on [Si II] 35 μm, Brγ, and the *IRAS* 60 + 100 μm fluxes. They may, however, contribute to the production of high-velocity H I (see later).

Given the difficulty in finding a satisfactory solution applying conventional physics, we have relaxed certain theoretical assumptions and investigated the properties of the new models. First, if we assume that *C* shocks persist but force the oxygen not locked in CO to stay atomic in a fast ($v_s \sim 40$ km s^{-1}) *C* shock (class F), we can find a single shock fit to the peak emission. However, the [O I] 63 μm/H_2 1–0 *S*(1) emission ratio is then very sensitive to the shock velocity, and we would therefore expect large variations from place to place—which are not observed.

The next assumption to be relaxed is that the shocks are *J*-type rather than *C*-type. Slow, nondissociative or partially dissociative *J* shocks are not expected on theoretical grounds; molecular shocks with these velocities are thought to form *C* shock configurations (see Hollenbach, Chernoff, and McKee 1989). Perhaps, however, the penetration of soft X-rays into the molecular cloud can raise the ion fraction in the molecular gas to sufficiently high values that 10–20 km s^{-1} shocks are *J*-type. Ignoring this theoretical difficulty does not by itself provide a good fit (class B). However, if the oxygen chemistry is also suppressed (so that atomic oxygen is preserved), we are able to find a single shock fit to the observations (model C). Although two questionable assumptions are involved in obtaining this fit, there are several positive features to such a model, as well as supporting evidence for such a shock in Orion: (*a*) the [O I] 63 μm to H_2 1–0 *S*(1) ratio is fairly constant as a function of shock velocity in the range $v_s \sim 10$–20 km s^{-1}; thus the model is somewhat robust and may explain the observed spatial correlation of [O I] 63 μm with H_2 1–0 *S*(1). (*b*) Dissociative or partially dissociative shocks might explain why the high-velocity atomic hydrogen is observed to be correlated with H_2 emission. (*c*) Partially dissociative shocks tend to produce rather constant ratios (~ 10) of 1–0 *S*(1)/2–1 *S*(1), as observed (Burton *et al.* 1988) and (*d*) Brand *et al.* (1988) and Burton *et al.* (1988*b*) have presented observational evidence that the detailed H_2 spectra for the BN-KL shock region of Orion are better fit by partially dissociative *J* shocks; therefore, there is circumstantial evidence for such slow *J* shocks in other regions.

A related issue, which has not been directly addressed by the modeling thus far, is explaining the H I emission. The presence of considerable quantities of high-velocity atomic gas displaying the same morphology as the shocked molecular hydrogen suggests that considerable dissociation has taken place (Burton *et al.* 1988). Since the relative fraction of H_2 and H I line emission varies with location in IC 443, it would suggest that the fraction of dissociated gas varies with position in the source. Yet a single, partially dissociating *J* shock picture such as class C would require a fine-tuned range of shock velocities over the entire region mapped in H_2 and H I to produce this result, since there is only a narrow range of shock velocities (of ~ 15 km s^{-1}) which partially dissociate H_2, leaving both significant quantities of atomic and molecular hydrogen. It is possible that fast, dissociative *J* shocks, such as class A, may contribute to the 21 cm emission, but the filling factor of such shocks must be small so as not to violate constraints such as the observed far-IR emission. It may also be possible that the H I was produced at an earlier epoch, when the shocks were mostly of the dissociating *J*-type, and that at present the shocks have decelerated to form *C*-type, or slow *J*-type shocks.

Though no completely satisfactory model has been found, some general conclusions regarding the physical parameters for the gas can be drawn. Preshock densities are high, at least 10^4 cm^{-3} in the best-fitting *C* shock models, rising to $\sim 10^5$ cm^{-3} in the *J* shock models. Shock velocities are generally less than ~ 40 km s^{-1}, with very few shocks moving as fast as ~ 100 km s^{-1}. Magnetic field strengths of order 100 μG are predicted, a nominal value for dense clouds, but these are not tightly constrained by the models. Elemental depletions from cosmic abundances (see Table 5) are generally as expected in molecular clouds, though again these are not tightly constrained. The nondetection of CO (22–21) may imply a lower carbon abundance than we assumed. The area filling factors of the shocks are high, at least 1–4, suggesting that shocked surfaces are curved and/or that there are many shocked clumps within each beam. This is consistent with the high gas density derived.

d) Further Observations

IC 443 has proven to be an interesting laboratory for studying interstellar shocks. Clearly, our theoretical understanding is not satisfactory and further effort is warranted. However, within the context of the current models, several additional observations are suggested which may help point the way to a better understanding of such shocks. The CO spectrum is predicted to be significant in both the *C* and *J* shock models for IC 443; the difference is that the *J* shock model has higher densities in the warm postshock gas, so that the higher rotational transitions of CO are more intense. Slow *C* shocks may show high ratios of [O I] 145 μm/63 μm. The [C I] (609, 370 μm) line emission is also particularly strong in slow *C* shocks. Fast *J* shocks, although almost certainly ruled out by the *IRAS* 60 + 100 μm observations, are predicted to have relatively strong [C II] 158 μm line emission.

It may be noted from Table 6 that the 0–0 *S*(13) line intensity is particularly sensitive to the shock parameters, being negligible in the slow *C* shock and appreciable in the partially dissociative *J* shock. This might suggest that this line is an excellent shock diagnostic. The 0–0 *S*(13) line, however, arises from a high rotational level of the hydrogen molecule. Many collisions are required to populate it, and thus the level population is extremely sensitive to the collision rates. These are poorly known at present; Burton *et al.* (1989*a*) show that very differ-

ent predictions for the line intensity can be obtained by using different cross sections taken from the astronomical literature. Therefore, unfortunately, this line cannot be used to place strong constraints on the models.

Whether one models the H_2 and O I line emission as arising from either a single shock (slow J or fast C), or from a combination of slow and fast C shocks, as discussed above, it would be quite surprising to find an exact correlation of [O I] and H_2 1–0 $S(1)$ over the entire source. In the former case, one would expect spatial variations in the shock velocity, and the ratio of [O I] to H_2 1–0 $S(1)$ is sensitive to v_s. In the latter case, one would expect spatial variations in the relative filling factors of the slow and fast C shocks and, therefore, variations in the [O I] 63 μm to H_2 1–0 $S(1)$ ratio. Further mapping of the [O I] 63 μm line is required. Higher spectral resolution studies of [O I] 63 μm would also be useful in determining whether a single shock produces both the H_2 and O I line emission; differences in either the line widths or the average velocities would suggest the presence of multiple shocks.

e) *Summary of Shock Modeling*

Until further observations can be made, as outlined above, we tentatively conclude that, based on our current understanding of shock physics, the most likely model is one in which a range of shock velocities is present in clumpy material, and that lower velocity C shocks produce the [O I] 63 μm line emission (class D) while higher velocity C shocks produce the H_2 line emission (class E). This requires, however, that the area filling factor of the slow and fast C shocks be similar all over the mapped region. Dissociative J shocks (class A) may be (or have been) present and may account for the observed high-velocity H I gas. However, they cannot contribute significantly to the emission without producing excessive grain continuum emission. If relaxing certain theoretical assumptions is permitted, then partially dissociative J shocks (class C) provide a good fit to the observations. It is not clear, however, why they would not be C shocks and how the oxygen chemistry is suppressed. Overall, the pressures required to drive any of these shocks are uncomfortably high, and the observed correlation of O I and H_2, and of H I and H_2, are not well understood.

VI. TOTAL SHOCK CONTRIBUTION TO FAR-INFRARED LUMINOSITY

It is clear that the total infrared emission from IC 443, including both near-IR line emission and that measured by *IRAS*, dominates the cooling compared to the optical and X-ray emission. This has also been found for other SNRs. For instance, in the Large Magellanic Cloud, Graham *et al.* (1987) show that IR cooling dominates the atomic cooling (through X-ray line emission) by a factor of ~ 10. This ratio, the IRX (IR to X-ray flux), is considerably greater than unity for a number of galactic remnants; for instance the young SNRs Cas A, Tycho, Kepler, and RCW 86, and also for adiabatic remnants such as IC 443, Puppis A, and the Cygnus Loop (Dwek *et al.* 1987). Braun and Strom (1986*b*) and Mufson *et al.* (1986) have modeled the far-IR emission from IC 443 and conclude that it is dominated by blackbody radiation from collisionally heated dust grains. In these models, the grains have been heated by the passage of the SN shock wave and reradiate the energy as far-IR continuum. Braun and Strom find a dust temperature of 90–95 K, whereas Mufson *et al.* determine a lower temperature of 40–45 K. This lower temperature arises from the inclusion of line emission by Mufson *et al.* from [Ne II] at 12.8 μm, [Fe II] at 26 μm, [Si II] at 34.8 μm and [O I] at 63 μm. The emission from these lines accounts for virtually all the *IRAS* 12 μm and 25 μm band emission, and about $\frac{1}{3}$ of the 60 μm band emission in the model. Their model for the line emission, however, is only an estimate based on extrapolation from the Hβ line flux in the optical lobes of the remnant, using the models of Raymond (1979). This covers only the shock waves in the optical filaments and does not include the molecular shock responsible for the extensive H_2 line emission.

It is clear from both the [O I] data and from our shock modeling that far-IR line emission from the molecular shock is an important contributor to the *IRAS* 60 and 100 μm band emission. For the models we presented, only in model A (fast, dissociative shock) did grain emission dominate the 60 + 100 μm bands—and this model was ruled out because *too much* grain emission would be produced if it were to account for the [O I] 63 μm line flux.

Estimating the contribution of line emission to the *IRAS* fluxes depends on the shock model assumed to best describe the emission. With "conventional" shock physics, applying the superposition of fast + slow C shock models (D + E), the [O I] 63 μm + H_2O will dominate the *IRAS* 60 + 100 μm bands, and grain emission will be negligible. In the 60 μm band, [O I] would account for $\sim 25\%$ of the *IRAS* flux (similar to the estimates made from the data) and H_2O for $\sim 75\%$. The 100 μm band will be dominated by H_2O line emission. If this model is valid, then *IRAS* gas made a first detection of the expected copious H_2O line emission from molecular shocks.

If, on the other hand, the slow J shock model with O-chemistry suppressed (model C) is applied, since it provides the best fit to the data, then [O I] 63 μm dominates the 60 μm band and CO lines dominate the 100 μm band. The dust continuum would only provide about 10% of the emission.

The present shock models are not exact enough to tell whether all the far-IR emission is line emission. The indication, however, from both the modeling and the data is that line emission is an important, and very possibly the dominant, contributor to the emission from IC 443 at all IR wavelengths. The contribution of thermal far-IR emission from collisionally heated dust grains in the shocked molecular region of the source is small by comparison. IC 443 is the first *IRAS* source discovered to be dominated by line emission.

VII. CONCLUSIONS

The fine-structure emission from the [O I] 63 μm line has been detected in the SNR IC 443. The emission correlates well with the distribution of line emission from shock-excited molecular hydrogen, and it is concluded that the line is shock excited. X-ray heating, or UV-heating from a photodissociation region, are ruled out as possible excitation mechanisms for the [O I] line emission. It is also clear that the [O I] 63 μm line is an important contributor to the total emission in the *IRAS* 60 μm band, perhaps 40%–75%, although an accurate estimate of its contribution cannot yet be made until a larger region is mapped.

We have attempted to shock model the line emission from IC 443. With our current understanding of shock physics, we find it can be modeled as a superposition of C shocks driven by a constant driving pressure, with the slower shocks providing the [O I] line emission and the faster shocks the H_2 line emission. However, the same filling factors of fast and slow shocks are required across the source, which seems unlikely. We do find that a slow, partially dissociating J shock can match the observations. However, two questionable theoretical assump-

tions are required: (1) that the shock is in fact *J*-type and not *C*-type, which would be expected for the conditions present, and (2) that the oxygen chemistry is suppressed so that oxygen remains in atomic form and does not get converted into H_2O. We can provide little theoretical rationale for these two assumptions; however, observational evidence favoring such a shock model for Orion has also been found (Brand *et al.* 1988). Several observations are suggested which may help to distinguish between the models investigated. The cooling of the SNR is dominated by emission in the infrared. The observations suggest that [O I] is an important contributor to the *IRAS* 60 μm band flux, and the modeling suggests that either H_2O or CO lines (depending on the model chosen) may provide a substantial part of the remaining 60 and 100 μm band fluxes. The contribution of thermal emission from dust grains is small by comparison with the total IR line emission. We suggest, therefore, that shocked line emission from molecular hydrogen, neutral oxygen, water and/or carbon monoxide dominates the emission at infrared wavelengths.

We are particularly grateful to Helen Walker, David Neufeld, and Michael McCollough for help in reducing the *IRAS* data and interpreting it. David Chernoff kindly supplied us with some new model runs. Jurgen Wolf provided considerable help both with the detectors and during the flight series. Sean Colgan performed a critical reading of the manuscript and made many valuable comments on it. We also thank the staff of the Kuiper Airborne Observatory for their support for making the observations possible. This work was done while MGB held a National Research Council NASA Ames Research Associateship. D. J. H. acknowledges the support of NASA RTOP 188-44-53 for the theoretical modeling of interstellar shocks.

REFERENCES

Brand, P. W. J. L., Moorhouse, A., Burton, M. G., Geballe, T. R., Bird, M., and Wade, R. 1988, *Ap. J. (Letters)*, **334**, L103.
Braun, R., and Strom, R. G. 1986*a*, *Astr. Ap. Suppl.*, **63**, 345.
———. 1986*b*, *Astr. Ap.*, **164**, 193.
Burton, M. G. 1987, *Quart. J.R.A.S.*, **28**, 269.
———. 1988, in *IAU Colloquium 101, Supernova Remnants and the Interstellar Medium*, ed. R. S. Roger and T. L. Landecker (Dordrecht: Kluwer), p. 399.
Burton, M. G., Brand, P. W. J. L., Geballe, T. R., and Webster, A. S. 1989*a*, *M.N.R.A.S.*, **236**, 409.
Burton, M. G., Brand, P. W. J. L., Moorhouse, A., and Geballe, T. R. 1989*b*, in *Infrared Spectroscopy in Astronomy*, ed. B. H. Kaldeich (ESA SP-290), p. 281.
Burton, M. G., Geballe, T. R., Brand, P. W. J. L., and Webster, A. S. 1988, *M.N.R.A.S.*, **231**, 617.
Burton, M. G., *et al.* 1990, in preparation.
Chernoff, D. F., Hollenbach, D. J., and McKee, C. F. 1982, *Ap. J. (Letters)*, **259**, L97.
Cornett, R. H., Chin, G., and Knapp, G. R. 1977, *Astr. Ap.*, **54**, 889.
DeNoyer, L. K. 1979*a*, *Ap. J. (Letters)*, **228**, L41.
———. 1979*b*, *Ap. J. (Letters)*, **232**, L165.
Draine, B. T. 1980, *Ap. J.*, **241**, 1021.
Draine, B. T., and Roberge, W. G. 1984, *Ap. J.*, **282**, 491.
Draine, B. T., Roberge, W. G., and Dalgarno, A. 1983, *Ap. J.*, **264**, 485.
Draine, B. T., and Woods, D. T. 1989, in *Infrared Spectroscopy in Astronomy*, ed. B. H. Kaldeich (ESA SP-290), p. 155.
Dwek, E., Petre, R., Szymkowiak, A., and Rice, W. L. 1987, *Ap. J. (Letters)*, **320**, L27.
Erickson, E. F., *et al.* 1985, in *Symposium on Airborne Astronomy*, ed. H. Thronson and E. Erickson (NASA Conf. Proc. 2353), p. 298.
Erickson, E. F., Knacke, R. F., Tokunaga, A. T., and Haas, M. R. 1981, *Ap. J.*, **245**, 148.
Erickson, E. F., Matthews, S., Augason, G. C., Houck, J. R., Rank, D. M., and Haas, M. R. 1984, *Proc. SPIE*, **509**, 129.
Erickson, W. C., and Mahoney, M. J. 1985, *Astr. Ap.*, **290**, 596.
Fesen, R. A., and Kirshner, R. P. 1980, *Ap. J.*, **242**, 1023.
Georgelin, Y. M. 1975, Ph.D. dissertation, Université de Provence, Marseille, France.
Graham, J. R., Evans, A., Albinson, J. S., Bode, M. F., and Meikle, W. P. S. 1987, *Ap. J.*, **319**, 126.
Hollenbach, D. J. 1982, *Ann. NY Acad. Sci.*, **395**, 242.
Hollenbach, D. J., Chernoff, D. F., and McKee, C. F. 1989, in *Infrared Spectroscopy in Astronomy*, ed. B. H. Kaldeich (ESA SP-290), p. 245.
Hollenbach, D. J., and McKee, C. F. 1989, *Ap. J.*, **342**, 306.
Hollenbach, D. J., and Shull, J. M. 1977, *Ap. J.*, **216**, 419.
Kwan, J. 1977, *Ap. J.*, **216**, 713.
London, R., McCray, R., and Chu, S-I. 1977, *Ap. J.*, **217**, 560.
Malina, R., Lampton, M., and Bowyer, S. 1976, *Astr. Ap.*, **207**, 894.
McKee, C. F., and Hollenbach, D. J. 1987, *Ap. J.*, **322**, 275.
Mufson, S. L., McCollough, M. L., Dickel, J. R., Petre, R., White, R., and Chevalier, R. 1986, *A.J.*, **92**, 1349.
Neufeld, D. A., and Melnick, G. J. 1987, *Ap. J.*, **322**, 266.
Petre, R., Canizares, C. R., Winkler, P. F., Seward, F. D., Willingale, R., Rolf, D., and Woods, N. 1983, in *IAU Symposium 101, Supernova Remnants and their X-ray Emission*, ed. J. Dazinger and P. Gorenstein (Dordrecht: Reidel), p. 289.
Petre, R., Szymkowiak, A. E., Seward, F. P., and Willingale, R. 1988, *Ap. J.*, **335**, 215.
Raymond, J. 1979, *Ap. J. Suppl.*, **39**, 1.
Thronson, H. A., *et al.* 1986, *A.J.*, **91**, 1350.
Tielens, A. G. G. M., and Hollenbach, D. 1985, *Ap. J.*, **291**, 722.
Wagner, A. F., and Graff, M. M. 1987, *Ap. J.*, **317**, 423.
Watson, M. G., Willingale, R., Pye, J. P., Rolf, D. P., Wood, N., Thomas, N., and Seward, F. D. 1983, in *IAU Symposium 101, Supernova Remnants and their X-ray Emission*, ed. J. Danziger and P. Gorenstein (Dordrecht: Reidel), p. 273.
Werner, M. W. 1982, *Ann. NY Acad. Sci.*, **395**, 79.
White, G. J., Rainey, R., Hayashi, S. S., and Kaifu, N. 1987, *Astr. Ap.*, **173**, 337.

MICHAEL G. BURTON, EDWIN F. ERICKSON, MICHAEL R. HAAS, and DAVID J. HOLLENBACH: NASA Ames Research Center, MS: 245-6, Moffett Field, CA 94035